

Effect of damage evolution of coal on permeability variation and analysis of gas outburst hazard with coal mining

Yi Xue^{1,2} · Feng Gao^{1,2} · Xingguang Liu³

Received: 8 May 2015 / Accepted: 24 June 2015 / Published online: 2 July 2015
© Springer Science+Business Media Dordrecht 2015

Abstract Coal and gas outburst disasters in coal seams are becoming more serious as coal mines extend deeper underground in China. Damage evolution has affected gas flow in coal seam greatly, which also controls gas permeation and gas extraction results, and finally, it has tremendous influence on prevention and control of gas disaster accidents. In this paper, the cracking process of coal under compressive stress condition and the permeability variation during the whole process is experimentally studied with the aid of 3D acoustic emission monitoring system. The experimental results suggest that the coal failure and degradation of mechanical properties are essentially related to the propagation and coalescence of induced cracks. Using a damage tensor defined by the direction-dependent crack density, the damage evolution during the whole loading process is studied. It is revealed that the damage evolution is mainly initiated with the appearance of microcracks and accelerated in the post-peak region. During the post-peak region, a similar increase tendency of damage and permeability is noticed, and therefore, a post-peak permeability model is proposed considering the influence of damage evolution on the permeability variation in the post-peak region. Finally, we analyze the gas outburst hazard with coal mining. There exists a transition zone around the vertical stress concentration, and energetic failure may result in this transition zone.

Keywords Gas outburst hazard · Permeability variation · Damage · Permeability enhanced coefficient

✉ Feng Gao
fgao@cumt.edu.cn

Yi Xue
xueyixy@126.com

¹ State Key Laboratory for Geomechanics and Deep Underground Engineering, China University of Mining and Technology, Xuzhou 221008, China

² School of Mechanics and Civil Engineering, China University of Mining and Technology, Xuzhou 221008, China

³ College of Sciences, Shandong University of Sciences and Technology, Qingdao 266510, China

1 Introduction

The rapid development of China's economy has a huge demand for coal resources, and coal production has increased with an average annual growth rate of 10 % in the past decade. With the increase in mining depth and the development of coal mining mechanization, coal mine accidents still occur frequently, especially for gas disaster. The data indicate that the proportion of gas disaster reaches to as high as 50.8 % among all coal mine accidents in China in 2012 (Pan et al. 2014; Li 2014; Lu et al. 2014; Meng et al. 2015; Wang et al. 2014; Yu et al. 2014). Therefore, the gas disaster is an urgent problem which needs to be solved. The excavation processes severely disequilibrate the initial balance state of geological stresses of coal seam, resulting in the further extension of fractures and gas emission. If the gas emissions cannot be effectively controlled, the gas content in the working space may exceed the limit for safety working conditions. This may stop working process or cause the gas explosion in the working space or the occurrence of coal and gas outburst accident (Karacan 2007). Different measures are taken to reduce this gas disaster, for example in-seam gas pre-drainage ahead of mine development (Karacan et al. 2011), hydraulic fracturing (Huang et al. 2011), and high-pressure waterjet techniques (Aguado and Gonzalez 2007; Lu et al. 2011).

The causes of instantaneous gas outbursts are complex, and a spatial variation in stresses, gas pressures, damage, permeability, and desorption rate exists ahead of the mining face in underground coal seams. This is due mainly to the sudden stress redistribution induced by mining (Harpalani 1985). Changes in one zone influence adjacent zones and are of great consequence in controlling the stability of coal seams. Therefore, an understanding of the damage evolution law and permeability variation is important in this process. Experimental measurements of these effects are crucial in understanding the response where the coal seam ahead of the mining face is loaded.

To date, many experimental and numerical investigations have been conducted to study the gas flow through fractured rocks. Measurements on coal have investigated the evolution of strength and the stress–strain characteristics in triaxial compression (Gentzis et al. 2007; Hobbs 1964; Medhurst and Brown 1998), scale effects on strength (Medhurst and Brown 1998; Bieniawski 1968; Scholtes et al. 2009), the evolution of elastic parameters (Kaiser and Maloney 1982), the influence of width/height ratio on post-failure behavior (Das 1986), and the dependence on loading rate (Okubo et al. 2006). Permeability of intact coal has been studied as a function of applied stress (Liu et al. 2011; Pini et al. 2009; Siriwardane et al. 2009; Wang et al. 2011; Wang et al. 2013), of pore pressure, and of fluid composition (Harpalani and Chen 1997; Harpalani and Schraufnagel 1990). Nonetheless, little work is available to quantitatively characterize the influence of the interior fracture or damage evolution on gas transport properties of fractured coal in the post-peak region. Generally, with the progressive loading, coal fracturing generates new fracture surfaces, accelerates the gas desorption, releases internal energy, and may promote a feedback to runaway failure. This highlights the importance of understanding the relationship between progressive damage and permeability evolution.

The purpose of this paper was therefore to characterize the damage evolution process of coal under compressive stress condition and to study its effect on the permeation properties of damaged coal. The three-dimensional acoustic emission (AE) technique, which is an ideal nondestructive method for studying crack growth (damage) at its actual state, is used to detect the changes in the interior fracture of coal. In the paper, using the experimental data and an anisotropic damage tensor proposed by Shao et al. (2006), the damage evolution law of coal under compressive stress condition was discussed. Then, we analyzed the

characterization of permeability variation. A post-peak permeability model was proposed to describe the influence of damage evolution on permeability variation during the post-peak process based on the permeability model proposed by Cui and Bustin (2005). Finally, based on the experimental observation, we analyze the gas outburst hazard with coal mining. There exists a transition around the vertical stress concentration, and energetic failure may result in this transition zone.

2 Design of the experimental tests

2.1 Testing facilities

The mechanical and permeability tests were conducted in Sichuan University in China with the MTS815 rock mechanics test system with a maximum axial loading capacity of 4600 kN. Two linear variable differential transducers and an axial extensometer (−2.5 to 5 mm) are used to measure the axial deformation, while the circumferential deformation is measured by an extensometer (−2.5 to 8 mm).

Meanwhile, a 3D acoustic emission system (PCI-2) is used to record the cracking process. In the test, eight sensors were attached to specimen to obtain the spatial distribution of AE events, and the sampling rate was 40 m/s. The used AE sensors are Mic30 sensors with a central frequency of 300 kHz and a frequency range from 150 to 1000 kHz. The preamplifier gain is 40 dB, and the threshold is fixed at 30 dB. The average compressive wave velocity is about 5200 m/s (range 5120–5351 m/s).

The coal samples used in the experiment were chosen from No. 8 Coal Mine of Pingdingshan, Henan Province, China. The coal samples were further processed into cylinders of 50 mm diameter and 100 mm length. The gas was 99.9 % pure methane. The confining pressure was set at 10 MPa, and the gas pressure was set at 1, 2, and 3 MPa, respectively.

2.2 Test method

The experimental procedure was as follows: (1) The sample was placed on the testing machine, and then, hydrostatic pressure was applied to the coal sample to 10 MPa at 3 MPa/min. (2) Methane was gradually injected to increase the pressure with an increment of 0.25 MPa. After reaching the setting pressure (1, 2, 3 MPa), the pressure at the inlet end was maintained stable. Once the methane was completely adsorbed, the valve at the outlet end was opened, and its pressure was maintained at 0.1 MPa; when the gas flow was stable, the initial gas flow was recorded. (3) The confining pressure was maintained constant, and the force control mode was used to load the axial pressure at a speed of 10 kN/min. In the post-peak region, the displacement control mode was used and the loading speed was 0.04 mm/min. (4) When the load reached a certain state, the outlet end was opened, and the gas flow was recorded. After that, the outlet end was closed, and the load was continued. (5) When the coal sample reached the residual stage, the test was concluded, and the above steps were repeated with next sample.

The gas permeability is defined by Darcy's equation as follows:

$$k = \frac{2Q_0 P_0 \mu L}{A(P_1^2 - P_2^2)} \quad (1)$$

where k is the gas permeability (m^2), Q_0 is the volumetric flow rate at the reference pressure (m^3/s), μ is the gas viscosity ($\text{Pa} \cdot \text{s}$), L is the length of the coal sample (m), P_0 is

the reference pressure (Pa), A is the cross-sectional area of the coal sample (m^2), P_1 is the upstream gas pressure, (Pa), and P_2 is the downstream gas pressure (Pa).

3 Theoretical background of data interpretation

In the last decades, numerous damage models are proposed to describe the mechanical behavior of damaged rock by the induced cracks (Kachanov 1994; Ju 1990). The degradation of mechanical properties is essentially related to the direction-dependent crack density (Kachanov 1994). In this study, an anisotropic damage tensor proposed by Shao et al. (2006) is employed to estimate the damage variation in coal under compressive stress condition. The brief review of the damage tensor and its determination method with the mechanical tests is given in this section.

The authors consider a representative element volume containing randomly distributed penny-shape microcracks. It is assumed that the brittle materials are subjected to compression-dominated stresses. The crack density remains small, and the interaction between microcracks can be neglected before the onset of the coalescence of microcracks. The initial behavior of material is isotropic, and anisotropy is fully induced by preferential distribution of microcracks.

Based on the micromechanical study, the free enthalpy function W_c of the brittle material containing randomly distributed microcracks is obtained by the integration of the free enthalpy of each family of microcracks over all the space orientations on the surface of unit sphere, denoted by S^2 :

$$\begin{aligned}
 W_c = & \frac{1}{2} \boldsymbol{\sigma} : S^0 : \boldsymbol{\sigma} + \frac{h}{4\pi} \int_{S^{2+}} \omega(\vec{n}) \left(1 - \frac{\nu_0}{2}\right) \times (\boldsymbol{\sigma} \times \vec{n}) \times \langle \vec{n} \times \boldsymbol{\sigma} \times \vec{n} \rangle^+ \vec{n} dS \\
 & + \frac{h}{4\pi} \int_{S^2} \omega(\vec{n}) \{ (\boldsymbol{\sigma} \times \boldsymbol{\sigma}) : (\vec{n} \otimes \vec{n}) - \boldsymbol{\sigma} : (\vec{n} \otimes \vec{n} \otimes \vec{n} \otimes \vec{n}) : \boldsymbol{\sigma} \} dS
 \end{aligned}
 \tag{2}$$

where $\boldsymbol{\sigma}$, ν_0 , and S^0 represent the macroscopic stress tensor, poisson ratio, and the elastic compliance tensor of the undamaged material, respectively. The continuous crack density function $\omega(\vec{n})$ defines the crack density associated with the family of microcracks with normal unit \vec{n} . The sub-domain S^{2+} corresponds to the orientations of opened cracks (Pensee et al. 2002). The parameter $h = 16(1 - \nu_0^2)/(3E_0(2 - \nu_0))$ denotes the elastic compliance of a crack.

Then, a second-order damage tensor at macroscopic level, which is a function of crack density $\omega(\vec{n})$, is defined as

$$\mathbf{D} = \frac{1}{4\pi} \int_{S^2} \omega(\vec{n}) (\vec{n} \otimes \vec{n}) dS
 \tag{3}$$

Based on the previous work (Lubarda and Krajcinovic 1993; Yang et al. 2001), the crack density function $\omega(\vec{n})$ can be approximated by the macroscopic damage tensor, \mathbf{D} , as follows:

$$\omega(\vec{n}) = \frac{15}{2} \left[\mathbf{D} : (\vec{n} \otimes \vec{n}) - \frac{1}{5} tr \mathbf{D} \right]
 \tag{4}$$

On this basis, two particular cases are considered to obtain the analytical integration of the macroscopic free enthalpy function (Eq. 2) using the second-order damage tensor approximation (Eq. 4): In the first case, all the microcracks are opened ($S^{2+} \equiv S^2$), and in the second case, all the microcracks are closed ($S^{2+} \equiv \emptyset$). For these two situations, the macroscopic free enthalpy function is explicitly expressed with the second-order damage tensor \mathbf{D} by the making the integration of Eq. (2) over the space orientations S^2 :

$$W_c = \frac{1}{2} \boldsymbol{\sigma} : S^0 : \boldsymbol{\sigma} + a_1 \text{tr} \mathbf{D} (\text{tr} \boldsymbol{\sigma})^2 + a_2 \text{tr} (\boldsymbol{\sigma} \times \boldsymbol{\sigma} \times \mathbf{D}) + a_3 \text{tr} \boldsymbol{\sigma} \text{tr} (\mathbf{D} \times \boldsymbol{\sigma}) + a_4 \text{tr} \mathbf{D} \text{tr} (\boldsymbol{\sigma} \times \boldsymbol{\sigma}) \tag{5}$$

The four parameters a_i are given by

$$a_1 = \frac{-c}{70} h, \quad a_2 = \frac{7 + 2c}{7} h, \quad a_3 = \frac{c}{7} h, \quad a_4 = \frac{-c}{35} h \tag{6}$$

where the coefficient c is equal to $-v_0$ for the opened cracks and -2 for the closed cracks. This form of thermodynamic potential is similar to that used by Hayakawa and Murakami (1997) from a fully macroscopic assumption.

By making the standard derivation of the thermodynamic potential (Eq. 5), the stress–strain relation of the damaged material is obtained:

$$\begin{aligned} \boldsymbol{\varepsilon} - \boldsymbol{\varepsilon}^r(\mathbf{D}) &= \frac{\partial W_c(\boldsymbol{\sigma}, \mathbf{D})}{\partial \boldsymbol{\sigma}} = \frac{1 + v_0}{E_0} \boldsymbol{\sigma} - \frac{v_0}{E_0} (\text{tr} \boldsymbol{\sigma}) \boldsymbol{\delta} + 2a_1 (\text{tr} \mathbf{D} \text{tr} \boldsymbol{\sigma}) \boldsymbol{\delta} \\ &+ a_2 (\boldsymbol{\sigma} \times \mathbf{D} + \mathbf{D} \times \boldsymbol{\sigma}) + a_3 [\text{tr} (\boldsymbol{\sigma} \times \mathbf{D}) \boldsymbol{\delta} + (\text{tr} \boldsymbol{\sigma}) \mathbf{D}] + 2a_4 \text{tr}(\mathbf{D}) \boldsymbol{\sigma} \end{aligned} \tag{7}$$

where $\boldsymbol{\varepsilon}^r(\mathbf{D})$ represents the inelastic strain tensor induced by the sliding and misfit of induced cracks. $\boldsymbol{\delta}$ denotes the second-order unit tensor with the components being given by the Knocker’s symbol. The constitutive Eq. (7) can be rewritten in the following form:

$$\boldsymbol{\varepsilon} - \boldsymbol{\varepsilon}^r(\mathbf{D}) = \frac{\partial W_c(\boldsymbol{\sigma}, \mathbf{D})}{\partial \boldsymbol{\sigma}} = S(\mathbf{D}) : \boldsymbol{\sigma} \tag{8}$$

The components of the elastic compliance tensor of the damaged material, $S(\mathbf{D})$, are given by

$$\begin{aligned} S_{ijkl}(\mathbf{D}) &= \frac{1 + v_0}{2E_0} (\delta_{ik} \delta_{jl} + \delta_{il} \delta_{jk}) - \frac{v_0}{E_0} \delta_{ij} \delta_{kl} + 2a_1 (\text{tr} \mathbf{D}) \delta_{ij} \delta_{kl} \\ &+ \frac{1}{2} a_2 (\delta_{ik} D_{jl} + \delta_{il} D_{jk} + D_{ik} \delta_{jl} + D_{il} \delta_{jk}) + a_3 (\delta_{ij} D_{kl} + D_{ij} \delta_{kl}) \\ &+ a_4 (\text{tr} \mathbf{D}) (\delta_{ik} \delta_{jl} + \delta_{il} \delta_{jk}) \end{aligned} \tag{9}$$

Therefore, in the coordinates frame associated with the principal directions of damage tensor, the strain–stress relations can be expressed in the standard matrix form by using the Voigt notation:

$$\begin{pmatrix} \varepsilon_{11} \\ \varepsilon_{22} \\ \varepsilon_{33} \\ 2\varepsilon_{12} \\ 2\varepsilon_{23} \\ 2\varepsilon_{31} \end{pmatrix} = \begin{pmatrix} S_{11} & S_{12} & S_{13} & & & \\ S_{21} & S_{22} & S_{23} & & & \\ S_{31} & S_{32} & S_{33} & & & \\ & & & 1/G_{12} & & \\ & & & & 1/G_{23} & \\ & & & & & 1/G_{31} \end{pmatrix} \begin{pmatrix} \sigma_{11} \\ \sigma_{22} \\ \sigma_{33} \\ \sigma_{12} \\ \sigma_{23} \\ \sigma_{31} \end{pmatrix} \tag{10}$$

As mentioned previously, the triaxial loading tests are performed to characterize the degradation of elastic moduli and inelastic deformations. From Eq. (10), we have:

$$\varepsilon_1 = S_{11}\sigma_1 + (S_{12} + S_{13})\sigma_3 \quad (11)$$

$$\varepsilon_3 = S_{31}\sigma_1 + (S_{32} + S_{33})\sigma_3 \quad (12)$$

Because the confinement (σ_3) was kept constant during the test, the incremental constitutive relation in axial and lateral directions can be obtained by taking the derivative of Eqs. (11) and (12), $S_{11} = d\varepsilon_1/d\sigma_1$, $S_{31} = d\varepsilon_3/d\sigma_1$. Therefore, the components S_{11} and S_{31} of the elastic compliance tensor of damaged rock can be fixed with stress–strain curve during the whole process. The variable D_1 essentially corresponds to the influence of cracks with normal parallel to axial stress, while D_2 and D_3 represent the influence of cracks with normal perpendicular to axial stress. In view of the axisymmetric configuration and loading condition, a transversely isotropic damage tensor is adopted which implies $D_2 = D_3$. The coefficient c is equal to $-v_0$ for the opened cracks and -2 for the closed cracks. Then, with the relationship given in Eq. (9), the axial damage variable D_1 and the lateral damage variable D_3 can be accordingly determined.

4 Experimental results

4.1 Macroscopic mechanical behavior and characteristics of the recorded AE events

The stress–strain curves and the variation in recorded AE cumulative counts in the test at the gas pressure of 3 MPa are presented in Fig. 1. It is noticed that the recorded AE events are very limited at the beginning of loading process (phase I). Then, a steady increasing phase (phase II) is observed with the increase in axial stress, which corresponds to the initiation and propagation of microcracks. When the volumetric strain of the coal is compressed to an extremum, the inflection point in the volumetric strain curve emerges due to the sliding and the opening of the induced microcracks. Next, the cracking process is accelerated when the axial stress approaches the peak point (σ_p). As a result, the rock failure takes place soon after the occurrence of AE accelerating phase (phase III). In the post-peak region (phase IV), considerable AE events are also recorded after the rock failure, and then, the increasing tendency is reduced slightly. Considering the fact that macroscopic failure surface is already formed in the post-peak region, the recorded AE events in this region are mainly related to the sliding along the failure surface. In general, the transition point to the steady increasing phase of AE events can be considered as the microcrack initiation stress (σ_{ci}), while the accelerated point of AE events can be considered as the crack damage stress (σ_{cd}) (Cai et al. 2004).

Using the Geiger locating algorithm (Geiger 1912) which is based on least square method, we get the spatial location of acoustic emission source according to the time difference of P wave received by sensors in different positions. Figure 2 shows the AE locating results in coal sample during the whole process. The deviatoric stress ratios are listed above the AE locating figures. When the deviatoric stress ratio is below 80 %, AE location events are lacking and arbitrarily distributed in the coal sample. Afterward, there are more and more AE location events when the deviatoric stress ratio is above 80 %. Then, when the deviatoric stress ratio is between 90 and 100 %, a large number of acoustic

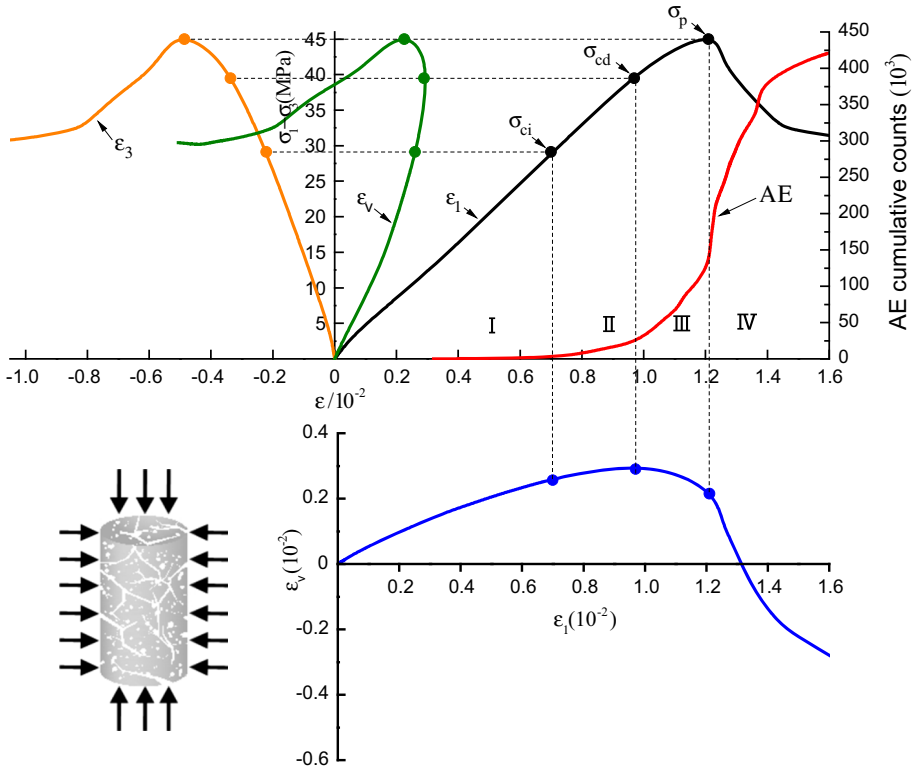
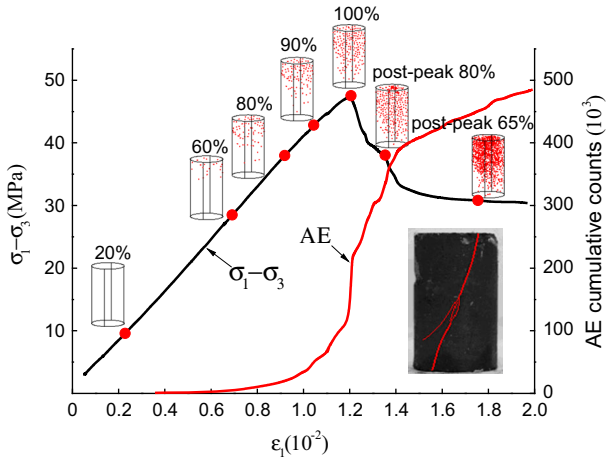


Fig. 1 Stress–strain curves and variation in AE cumulative counts of coal sample T1 under triaxial compression (gas pressure 3 MPa)

Fig. 2 Variation in AE cumulative counts with axial strain of coal sample T2 under triaxial compression (gas pressure 3 MPa)



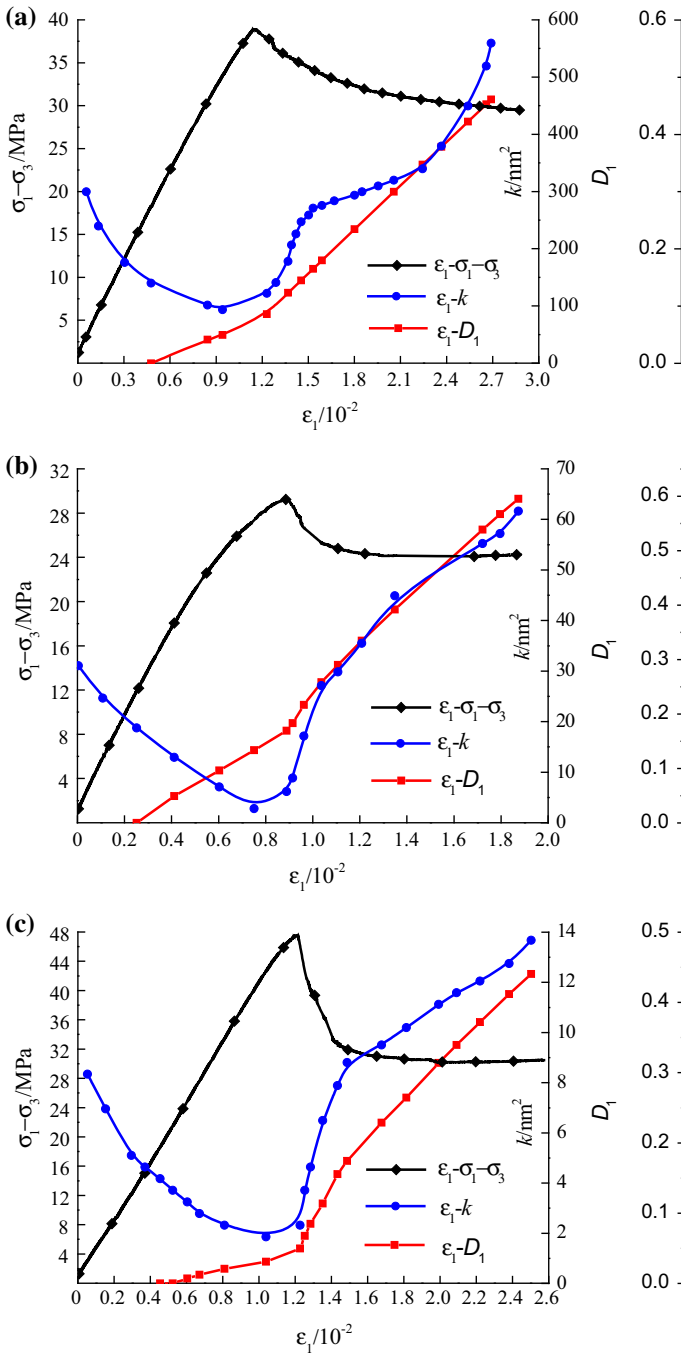


Fig. 3 Permeability and damage evolution curves of coal samples under different gas pressures: **a** sample W1 (gas pressure 1 MPa), **b** sample W2 (gas pressure 2 MPa), **c** sample W3 (gas pressure 3 MPa)

emission points are concentrated around the main crack surface. Compared with the deviatoric stress peak, the cumulative AE points in the coal samples increase greatly in quantity and distribution range when the deviatoric stress ratio reaches post-peak 80 % and post-peak 65 %.

4.2 Damage and permeability evolution tendency

With the method proposed in above section, the damage evolution of coal under compressive stress condition is determined. As the change in the permeability of coal sample is mainly determined by the axial stress and the permeability measured in the test is the axial permeability variation in the coal sample, we mainly analyze the influence of the axial damage evolution (D_1) on the permeability of the coal sample. The estimated damage variable and permeability during the whole process are drawn in Fig. 3.

In accordance with the AE characteristic, the damage variation is negligible at the beginning of loading process. Then, a steady increasing phase of damage is noticed due to the initiation of microcracks. Finally, with the propagation and coalescence of the microcracks, the increasing rate rises much further in post-peak region. Evidently, the damage evolution process is globally in accordance with the AE characteristics, and the degradation of mechanical properties of coal is essentially related with the cracking process.

The apparent permeability of damaged coal is obtained with Eq. (1). In Fig. 3, the permeability decreases with the increase in stress in the pre-peak region, while the permeability grows with the increase in damage during the rock failure and the post-peak region. During the post-peak region, a similar increase tendency of damage and permeability is noticed. The pronounced permeability increase takes place in the accelerated increasing phase of damage, due to the sliding and opening of the induced microcracks. Mainly affected by the initiation and coalescence of microcracks, the variation tendency between damage and permeability is in accordance with the post-peak region.

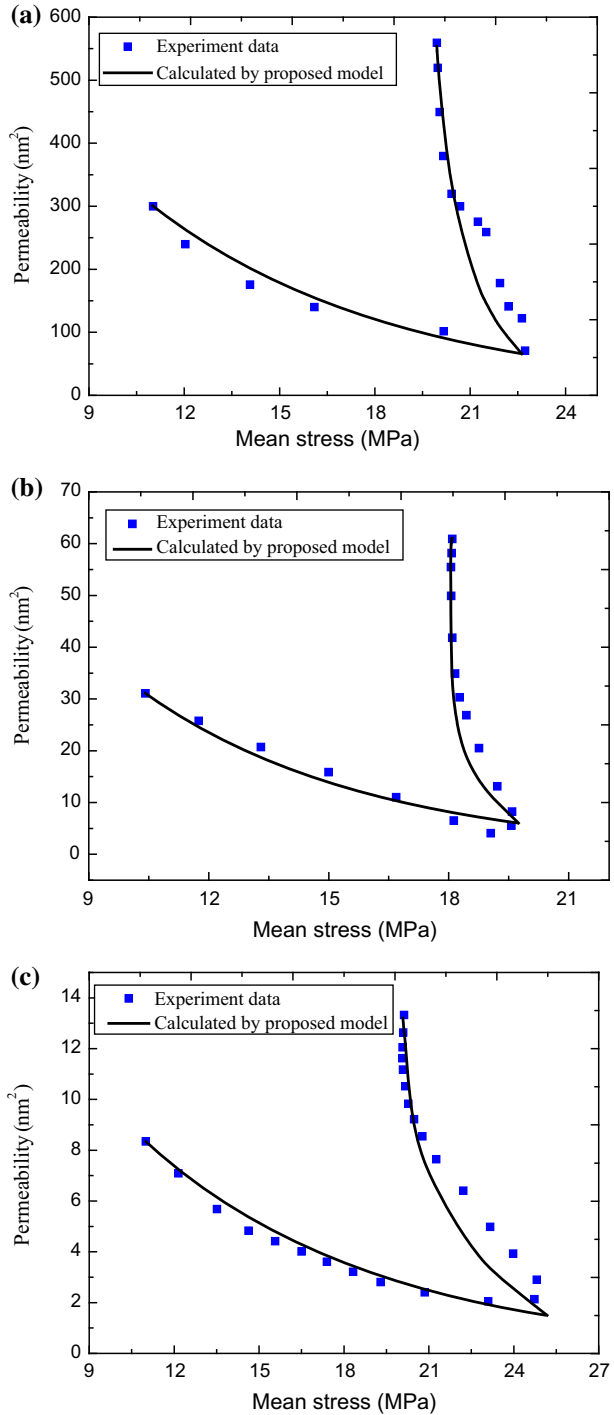
4.3 Impact of damage on the permeability of coal in the post-peak region

Based on the data analysis in previous section, it is noticed that there is a similar increase between permeability and damage variable in the post-peak region. In the post-peak region, the permeability of damaged rock increases with the increase in axial stress due to the open of microcracks. The crack is the main factor which controls the permeability of coal. Therefore, the damage variable defined by the crack density can be used to illustrate the characterization of permeability variation in coal in the post-peak region.

Based on field and laboratory data, extensive pre-peak permeability models were proposed based on the theory of poroelasticity or equivalent continuum approach, including Gilman and Beckie (2000), Seidle and Huitt (1995), Palmer and Mansoori (1998), Cui and Bustin (2005), Liu et al. (2010), and Xia et al. (2014). Cui and Bustin (2005) considered the influences of effective stresses and sorption-based volume changes, and illustrated the permeability variation with the change in stress in coal in the pre-peak region. Based on the stress-dependent permeability model proposed by Cui and Bustin (2005), we analyze the influence of the damage on permeability in the pre-peak region.

The authors regard coal as a porous medium, containing solid volume of V_s and pore volume of V_p . Its bulk volume is $V = V_p + V_s$, and its porosity is $\phi = V_p/V$. The volumetric strain and the pore-volume strain can be expressed by

Fig. 4 Comparison of model calculations with experimental data for permeability–stress curves of coal samples: **a** sample W1 (gas pressure 1 MPa), **b** sample W2 (gas pressure 2 MPa), **c** sample W3 (gas pressure 3 MPa)



$$\frac{\Delta V}{V} = -\frac{1}{K}(\sigma - \alpha p) + \varepsilon_s \tag{13}$$

$$\frac{\Delta V_p}{V_p} = -\frac{1}{K}(\sigma - \beta p) + \varepsilon_s \tag{14}$$

where $\beta = 1 - K_p/K_s$; K_p is the modulus of pores; ε_s is the sorption-induced volumetric strain.

Thus, the change in porosity of a deforming coal seam can be calculated by

$$d\phi = d\left(\frac{V_p}{V}\right) = \frac{V_p}{V} \left(\frac{dV_p}{V_p} - \frac{dV}{V}\right) \tag{15}$$

Integrating Eq. (15) yields:

$$\frac{\phi}{\phi_0} = \exp\left\{\left(\frac{1}{K} - \frac{1}{K_p}\right)[(\sigma - \sigma_0) - (p - p_0)]\right\} \tag{16}$$

A cubic law is applied to get the permeability by Cui and Bustin (2005)

$$k = k_0 \left(\frac{\phi}{\phi_0}\right)^3 = k_0 \exp\left\{3\left(\frac{1}{K} - \frac{1}{K_p}\right)[(\sigma - \sigma_0) - (p - p_0)]\right\} \tag{17}$$

which implicitly accounts for the effects of sorption-induced volumetric strain.

In the post-peak unloading process, the coal sample is further damaged. The internal fractures propagate and mutually communicate to form good gas flow channels. This increase in permeability under post-peak is mainly caused by the destruction of the coal and the propagation of cracks. Based on the data analysis in previous section, here we introduce an enhanced term $\gamma(d - d_0) + 1$ to Eq. (17) to describe the increase in permeability in the post-peak stage as

$$k = k_0 \times [\gamma(d - d_0) + 1] \times \exp\left\{3\left(\frac{1}{K} - \frac{1}{K_p}\right)[(\sigma - \sigma_0) - (p - p_0)]\right\} \tag{18}$$

where γ is the post-peak permeability enhanced coefficient, which reflects the degree of sensitivity of permeability to damage, $\gamma > 0$; d_0 is the damage value of coal in peak stress condition. With this equation, the permeability variation under post-peak region is obtained considering the influence of the damage variable D_1 .

The calculating results according to the permeability model proposed in this study are compared with the experimental data, as shown in Fig. 4. In the computation, the parameter $\frac{1}{K_p} - \frac{1}{K}$ is determined by numerical inversion of Eq. (17). The enhanced coefficient γ is obtained through the post-peak permeability model (Eq. 18). They are listed in Table 1. Although the values of the coefficient γ of these coal samples are approximately

Table 1 Calculating parameters for different samples in coal permeability experiments

Samples	Parameter	
	$\frac{1}{K_p} - \frac{1}{K}$ (GPa ⁻¹)	γ
W1	43.5	15
W2	58.5	16
W3	40.3	15

equal in this experiment, they may be different in other experiments. The coefficient γ is related to the physical property of coal, and the values of the coal samples chosen from the same mining area may vary within a certain range. Figure 4 shows that our model can well describe the experimental data. In the post-peak region, the generation of cracks weakens the mechanical properties of coal and accelerates the desorption rate, which is a complex process with the failure of coal. In this paper, we use a convenient and brief model to illustrate the permeability variation in the post-peak region.

5 Analysis of gas outburst hazard with coal mining

A schematic of this geometry (Fig. 5) represents the principal features of anticipated mining-induced changes in vertical stress, horizontal stress, pore pressure, permeability, and desorption rate. We use this to understand how these stress conditions and transport characteristics change with distance from the mining face and how these changes might contribute to failure. Immediately following excavation (at location a), the mining face is unconfined. With increasing distance from the face, horizontal stress gradually increases toward the initial in situ stress. The vertical stress increases rapidly with distance from the face due to the mining-induced stress abutment. Beyond location c, the vertical stress gradually resets to the in situ stress. In the zone between locations a and b, pore pressure in

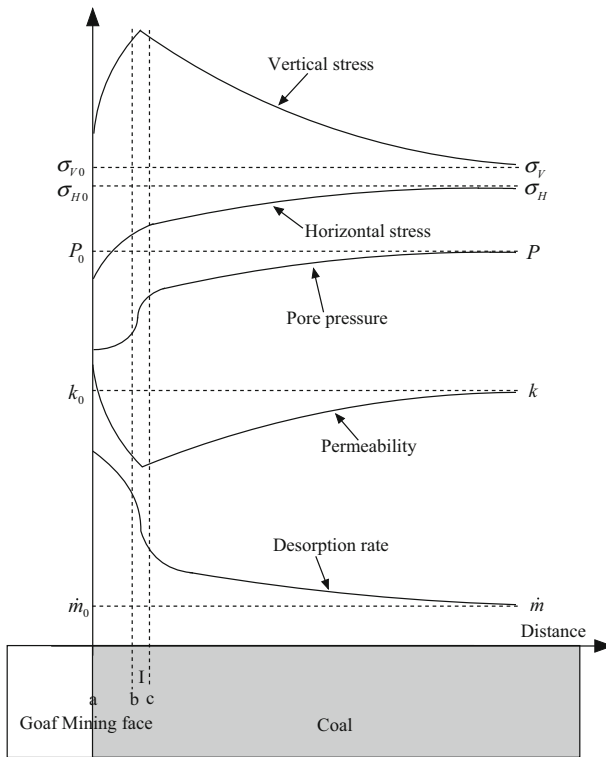


Fig. 5 Schematic diagram illustrating mining-induced stresses, pore pressure, permeability, and desorption rate ahead of the mining face

the fractures is small due to the high permeability, and the original pre-mining gas pressure may be reset rapidly between locations a and b. This increase in pore pressure decreases effective confining stress and hence has the potential to trigger failure in the coal. Between locations b and c, the permeability is below the initial permeability value due to the stress concentration, as found in this experimental study. Permeability is largest at the mining face since the coal is in the post-peak region. Beyond location c, permeability increases again with decreasing vertical stresses to its original value. The rate of desorption depends on the local pressure difference between the matrix and the fracture (Beamish and Crosdale 1998; Wang et al. 2013). On the mining face, the pore pressure in the matrix remains almost the same while the pore pressure in the fracture rapidly drops to zero. Thus, the maximum desorption rate occurs on the mining face where the largest pressure differential exists. With increasing distance from the face, this desorption rate decreases. This downward trend becomes significant between locations b and c, because the pore pressure in the fracture increases rapidly in this zone. Therefore, there exists a transition zone (zone I) considering the change in pore pressure, permeability and desorption rate, and the vertical stress concentration. The energy generated from gas expansion due to the desorption, together with the low permeability, microfracturing, and the fact that the coal is still under load, between locations b and c, has potentially significant weakening effects on the coal. Rapid, energetic failure may result in this transition zone.

With the above analysis, we may understand why techniques such as in-seam gas pre-drainage ahead of mine development (Karacan et al. 2011), hydraulic fracturing (Huang et al. 2011), and high-pressure waterjet techniques (Aguado and Gonzalez 2007; Lu et al. 2011) may suppress gas outbursts. The pre-drainage of gas reduces the pore pressure within coal seams, increases the effective confining stress, and hence tends to stabilize the coal seams. Hydraulic fracturing can enhance the permeability of coal seams, especially in the horizontal direction, so that gas can migrate rapidly and increases the effective stress accordingly.

6 Conclusions

In this study, under compressive stress condition, the damage evolution law and the characterization of permeability variation of coal are systematically studied. According to the analysis of experimental data and recorded AE events, it is confirmed that the permeability properties of damaged rock are strongly influenced by the initiation and growth of microcracks. Some principal conclusions are drawn as follows:

According to the recorded AE events, the damage evolution is rather limited at the beginning of loading process and is accelerated in the post-peak region due to the propagation and coalescence of induced microcracks. The permeability variation is essentially related to the damage evolution, and the similar variation tendency is noticed between damage and permeability during the post-peak process. Based on the analysis of experimental data, a post-peak permeability model is proposed considering the influence of damage evolution on the permeability variation in the post-peak region. By the comparison between numerical and experimental results, the post-peak permeability model is found to be capable to well reproduce the permeability variation with damage in the post-peak region. Based on the experimental observation, we analyze the gas outburst hazard with coal mining. There exists a transition zone of pore pressure, permeability, and desorption rate around the vertical stress concentration, and energetic failure may result in this transition zone.

Acknowledgments The authors are grateful to the financial support from the National Natural Science Foundation of China (No. 2011CB201205) and the Jiangsu Creative and Innovation fund for 2014 team projects.

References

- Aguado MBD, Gonzalez Nicieza C (2007) Control and prevention of gas outbursts in coal mines, Riosa–Olloniego coalfield Spain. *Int J Coal Geol* 69(4):253–266
- Beamish BB, Crosdale PJ (1998) Instantaneous outbursts in underground coal mines: an overview and association with coal type. *Int J Coal Geol* 35(1):27–55
- Bieniawski ZT (1968) The effect of specimen size on compressive strength of coal. *Int J Rock Mech Min Sci Geomech Abstr* 5(4):325–335
- Cai M, Kaiser PK, Tasaka Y, Maejima T, Morioka H, Minami M (2004) Generalized crack initiation and crack damage stress thresholds of brittle rock masses near underground excavations. *Int J Rock Mech Min Sci* 41:833–847
- Cui X, Bustin RM (2005) Volumetric strain associated with methane desorption and its impact on coalbed gas production from deep coal seams. *AAPG Bull* 89(9):1181–1202
- Das MN (1986) Influence of width/height ratio on post–failure behaviour of coal. *Int J Min Geol Eng* 4(1):79–87
- Geiger L (1912) Probability method for the determination of earthquake epicenters from the arrival time only. *Saint Louis Univ Bull* 8:60–71
- Gentzis T, Deisman N, Chalaturnyk RJ (2007) Geomechanical properties and permeability of coals from the Foothills and Mountain regions of western Canada. *Int J Coal Geol* 69(3):153–164
- Gilman A, Beckie R (2000) Flow of coal-bed methane to a gallery. *Transp Porous Media* 41(1):1–16
- Harpalani S (1985) Gas Flow through Stressed Coal. PhD thesis, University of California, Berkeley
- Harpalani S, Chen G (1997) Influence of gas production induced volumetric strain on permeability of coal. *Geotech Geol Eng* 15:303–325
- Harpalani S, Schraufnagel RA (1990) Shrinkage of coal matrix with release of gas and its impact on permeability of coal. *Fuel* 69:551–556
- Hayakawa K, Murakami S (1997) Thermodynamical modeling of elastic–plastic damage and experimental validation of damage potential. *Int J Damage Mech* 6:333–363
- Hobbs DW (1964) The strength and the stress–strain characteristics of coal in triaxial compression. *J Geol* 72:214–231
- Huang B, Liu C, Fu J, Guan H (2011) Hydraulic fracturing after water pressure control blasting for increased fracturing. *Int J Rock Mech Min Sci* 48(6):976–983
- Ju J (1990) Isotropic and anisotropic damage variables in continuum damage mechanics. *J Eng Mech* 116(12):2764–2770
- Kachanov M (1994) Elastic solids with many cracks and related problems. *Adv Appl Mech* 30:256–426
- Kaiser PK, Maloney SM (1982) Deformation properties of a sub–bituminous coal mass. *Int J Rock Mech Min Sci* 19:247–252
- Karacan CO (2007) Development and application of reservoir models and artificial neural networks for optimizing ventilation air requirements in development mining of coal seams. *Int J Coal Geol* 72(3):221–239
- Karacan CO, Ruiz FA, Cote M, Phipps S (2011) Coal mine methane: a review of capture and utilization practices with benefits to mining safety and to greenhouse gas reduction. *Int J Coal Geol* 86(2):121–156
- Li D (2014) Mining thin sub-layer as self-protective coal seam to reduce the danger of coal and gas outburst. *Nat Hazards* 71(1):41–52
- Liu J, Chen Z, Elsworth D, Miao X, Mao X (2010) Linking gas-sorption induced changes in coal permeability to directional strains through a modulus reduction ratio. *Int J Coal Geol* 83(1):21–30
- Liu J, Chen Z, Elsworth D, Qu H, Chen D (2011) Interactions of multiple processes during CBM extraction: a critical review. *Int J Coal Geol* 87:175–189
- Lu T, Zhao Z, Hu H (2011) Improving the gate road development rate and reducing outburst occurrences using the waterjet technique in high gas content outburst–prone soft coal seam. *Int J Rock Mech Min Sci* 48(8):1271–1282
- Lu S, Cheng Y, Ma J, Zhang Y (2014) Application of in-seam directional drilling technology for gas drainage with benefits to gas outburst control and greenhouse gas reductions in Daning coal mine, China. *Nat Hazards* 73(3):1419–1437

- Lubarda VA, Krajcinovic D (1993) Damage tensors and the crack density distribution. *Int J Solids Struct* 30(20):2859–2877
- Medhurst TP, Brown ET (1998) A study of the mechanical behaviour of coal for pillar design. *Int J Rock Mech Min Sci* 35(8):1087–1105
- Meng J, Nie B, Zhao B, Ma Y (2015) Study on law of raw coal seepage during loading process at different gas pressures. *Int J Min Sci Technol* 25(1):31–35
- Okubo S, Fukui K, Qi Q (2006) Uniaxial compression and tension tests of anthracite and loading rate dependence of peak strength. *Int J Coal Geol* 68(3):196–204
- Palmer I, Mansoori J (1998) How permeability depends on stress and pore pressure in coalbeds: a new model. *SPE Reservoir Eval Eng* 12:539–544
- Pan RK, Cheng YP, Yuan L, Yu MG, Dong J (2014) Effect of bedding structural diversity of coal on permeability evolution and gas disasters control with coal mining. *Nat Hazards* 73(2):531–546
- Pensee V, Kondo D, Dormieux L (2002) Micromechanics analysis of anisotropic damage in brittle materials. *J Eng Mech* 128(8):889–897
- Pini R, Ottiger S, Burlini L, Storti G, Mazzotti M (2009) Role of adsorption and swelling on the dynamics of gas injection in coal. *J Geophys Res Atmos* 114:B04203
- Scholtes L, Donz F-V, Khanal M (2009) Scale effects on strength of geomaterials, case study: coal. *J Mech Phys Solids* 59:1131–1146
- Seidle JR, Huiatt LG (1995) Experimental measurement of coal matrix shrinkage due to gas desorption and implications for cleat permeability increases. In: *Proceedings of the international meeting on petroleum engineering, Beijing*, pp 14–17, paper SPE30010
- Shao JF, Chau KT, Feng XT (2006) Modeling of anisotropic damage and creep deformation in brittle rocks. *Int J Rock Mech Min Sci* 43:582–592
- Siriwardane H, Haljasmaa I, McLendon R, Irdi G, Soong Y, Bromhal G (2009) Influence of carbon dioxide on coal permeability determined by pressure transient methods. *Int J Coal Geol* 77:109–118
- Wang S, Elsworth D, Liu J (2011) Permeability evolution in fractured coal: the roles of fracture geometry and water-content. *Int J Coal Geol* 87:13–25
- Wang S, Elsworth D, Liu J (2013) Permeability evolution during progressive deformation of intact coal and implications for instability in underground coal seams. *Int J Rock Mech Min Sci* 58:34–45
- Wang C, Wang C, Wei M, Gong B, Tan Y (2014) Deformation transition of intact coal induced by gas injection. *Int J Min Sci Technol* 24(6):833–838
- Xia T, Zhou F, Liu J, Gao F (2014) Evaluation of the pre-drained coal seam gas quality. *Fuel* 130:296–305
- Yang Q, Li Z, Tham LG (2001) An explicit expression of the second-order fabric tensor dependent elastic compliance tensor. *Mech Res Commun* 28(3):255–260
- Yu Y, Bai J, Wang X, Wang J, Xue S, Xu K (2014) High-resistance controlled yielding supporting technique in deep-well oil shale roadways. *Int J Min Sci Technol* 24(2):229–236